Journal of Magnetism and Magnetic Materials 554 (2022) 169301

Contents lists available at ScienceDirect

Journal of Magnetism and Magnetic Materials

journal homepage: www.elsevier.com/locate/jmmm

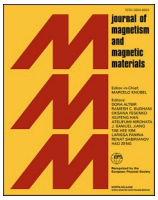

A method to compensate for the lift off effect of ACFM in crack estimation of nonferromagnetic metals

Shuxiang Zhao [a,b,c], Ying Shen [a,b,c], Lingsi Sun [d], Jiazeng Wang [a,b,c], Zhineng Mao [a,b,c], Zhaoqiang Chu [a,b,c], Jiamin Chen [e], Junqi Gao [a,b,c,*]

[a] Acoustic Science and Technology Laboratory, Harbin Engineering University, Harbin, 150001, China
[b] Key Laboratory of Marine Information Acquisition and Security (Harbin Engineering University), Ministry of Industry and Information Technology, Harbin, 150001, China
[c] College of Underwater Acoustic Engineering, Harbin Engineering University, Harbin, 150001, China
[d] Huazhong University of Science and Technology, 1037 Luoyu Road, 430074, Wuhan, China
[e] State Key Laboratory of Transducer Technology, Aerospace Information Research Institute, CAS, Beijing, China

ARTICLE INFO

Keywords:
Lift-off effect
Compensation method
ACFM
Aluminum plate
Crack estimation

ABSTRACT

Alternating current field measurement (ACFM) is one of the most important techniques for detecting metal cracks. During measurement, however, the changes in lift-off distance caused by coating corrosion and irregularity of the surface greatly affect the accuracy of crack sizing. To overcome this drawback, an advanced algorithm is proposed in this paper to compensate for the lift-off effect. Benefitting from this method, the dimensions of cracks can be inversed directly without considering the lift-off distance. More importantly, the algorithm has been verified efficiently as estimating the cracks of an aluminum workpiece. The results show that the sizing errors based on this algorithm can be limited to 10%.

1. Introduction

Nondestructive testing and evaluation (NDT&E) is important for the real-time inspection of working apparatuses and equipment maintenance, especially for accident reduction and operator safety. Compared with ultrasonic, thermal and optical methods, the electromagnetic method is preferable in the scenario of conductive structure detection for convenience and inexpensiveness. Alternating current field measurement (ACFM) has many merits against other electromagnetic NDT methods, including noncontact, no surface cleaning and efficiency. ACFM has been widely employed in many areas, such as petrochemicals [1], aviation [2], nuclear power plants [3] and railway transportation [4]. In addition, ACFM is able to quantify defects precisely, which is a significant advantage.

In detail, ACFM is a nondestructive electromagnetic inspection technology based on Faraday's induction law [5]. The working principle of ACFM is similar to eddy current testing (ECT). However, the ACFM usually uses magnetic sensors to detect magnetic field signals induced by defects instead of inductance coils used in ECT, such as anisotropic magneto-resistive (AMR) sensors, giant magneto-resistive (GMR) sensors and tunneling magneto-resistive (TMR) sensors [6].

Much attention has been focused on research on crack sizing taking advantage of ACFM technology due to its innate characteristics. Feng designed an ACFM probe to detect inner cracks of pipelines in terms of simulation results [7]. Yuan evaluated both inner and outer cracks of aluminum tubes using the ACFM method with double frequency excitation [8]. Ge realized the quantification of crack colonies by an algorithm of approximate decomposition [9]. Although cracks can be quantified precisely in various studies [10–14], including the aforementioned ones, they all have a common precondition, namely, the lift-off distance is consistent in the detection procedure. In ECT and ACFM, the lift-off distance defined as the space between the magnetic sensor and the workpiece surface is a significant parameter that can greatly affect the detection accuracy. During practical testing, the variations in the lift-off distance are mainly from the corrosion of the coating, irregular workpiece surface or detection device vibration. Thus, the compensation of the lift-off effect has attracted much interest in the field of electromagnetic inspection. Previously, there have been many studies on alleviating the lift-off effect in ECT [15–17]. Unfortunately, these methods can not be applied to ACFM directly, and very few reports concern the lift-off effect in this field. Amineh proposed a model-based inversion method to quantify cracks using ACFM data at arbitrary lift-

* Corresponding author.
E-mail address: gaojunqi@hrbeu.edu.cn (J. Gao).

https://doi.org/10.1016/j.jmmm.2022.169301
Received 15 February 2022; Received in revised form 17 March 2022; Accepted 21 March 2022
Available online 24 March 2022

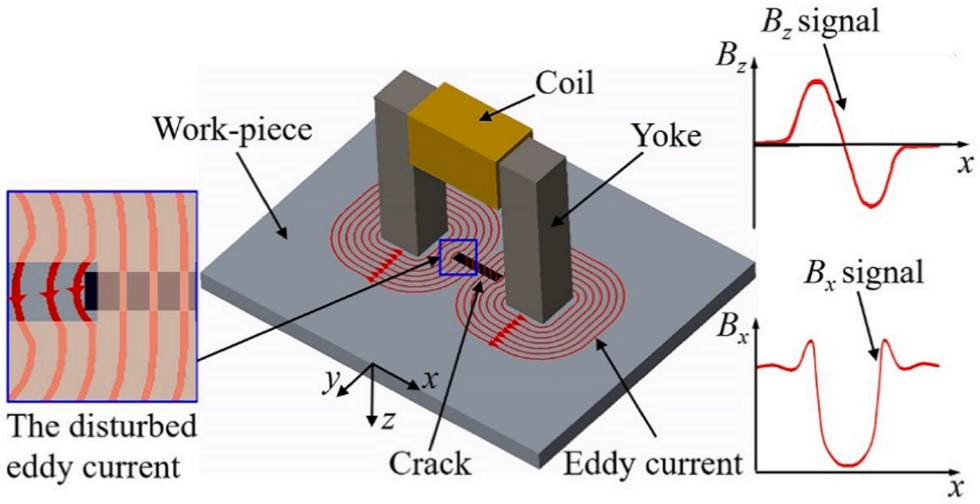

Fig. 1. Principle of ACFM for crack detection.

off distances [18], but the calculation was tremendously complicated. Therefore, it is necessary to find a relatively simple method that can measure defects under different lift-off distances in the ACFM detection system. This paper aims to predict the dimensions of unknown cracks overcoming the limitation of the lift-off distance.

The rest of the paper is organized as follows: first, the physical principle and theoretical model of eddy current induced by a crack are introduced in Section 2; second, a detailed description of the testing system, lift-off effect compensation procedure and crack inversion algorithm are provided in Section 3; subsequently, the experimental results of the developed method in terms of various lift-off distances are presented in Section 4; finally, the conclusions and possible future work are summarized in Section 5.

2. Theoretical analysis

2.1. ACFM principle

As shown in Fig. 1, an alternating current (AC) signal $y = Asin(\omega t + \varphi)$ is applied to a driving coil of a U-shaped probe. A is the amplitude of the current, ω is the angular frequency and φ is the starting phase angle. The magnetic permeability of U-shaped yoke is very large, and the yoke can capture more magnetic flux. When the driving magnetic field from the two legs of the U-shaped probe arrives at the surface of the conductive metal, the induced eddy current is excited in the metal. In detail, the current is mostly confined to the surface of the metal owing to the skin effect. The penetration depth of the induced current δ is given by Eq. (1).

$$\delta = \frac{1}{\sqrt{\pi f \mu_0 \mu_r \sigma}} \tag{1}$$

where $f = \omega/2\pi$ is the frequency of the driving signal, μ_0 is the air magnetic permeability,μ_r denotes the relative magnetic permeability and σ denotes the conductivity of the medium.

The induced current is approximately uniform between the two legs of the probe due to the unique structure of U-shaped. As illustrated in Fig. 1, the uniform current is disturbed by a crack. Eddy current flows down to the bottom of crack along vertical direction (z-axis), which corresponds to the variation of x direction magnetic density B_x. The crack depth can be quantified according to the perturbation of the B_x curve. Two peaks of z direction magnetic density B_z refer to the deviated current bypasses the two ends of target crack, and their polarities are reversed due to induced current flows in opposite directions at two ends of the crack. The distance between peak and trough in B_z is always

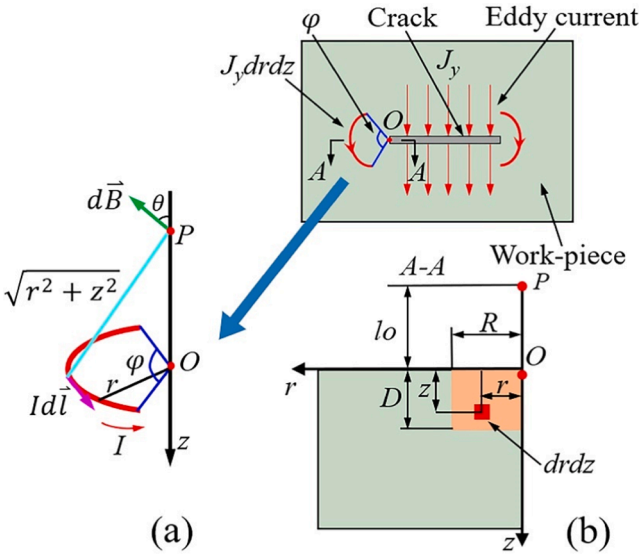

Fig. 2. (a) Unclosed circular coil axial magnetic field. (b) Mathematical model of the B_z signal with unknown lift off in ACFM detection.

adopted to indicate the crack length in conventional ACFM technique. Moreover, B_z signal waveform can also be used to estimate the crack depth according to our previous research [19].

The deflecting current of crack ends corresponding to the peak value of the B_z signal is studied alone, as shown in the partially enlarged view of Fig. 1. The induced current rotates with a nearby point of the crack end. For the convenience of calculations, we simplify the mode as circling motion. The distribution of the induced current along the depth direction of the crack, i.e., the z-axis, can be expressed as Eq. (2) [20] based on Maxwell equations.

$$J_y^z = J_y^0 e^{-z\sqrt{\pi f \mu \sigma}} \cos(\omega t - z\sqrt{\pi f \mu \sigma}) \tag{2}$$

where J_y^z denotes the y-component of electrical current density J traveling in the z-direction, J_y^0 is the value of J_y^z at $z = 0$, z is the coordinate position on the z-axis, and μ denotes the medium permeability, which is the product of μ_0 and μ_r.

According to Eq. (2), J_y^z declines exponentially with increasing distance between the target position and the surface of the conductor. The induced current can be disturbed to bring about the B_z signal vibration

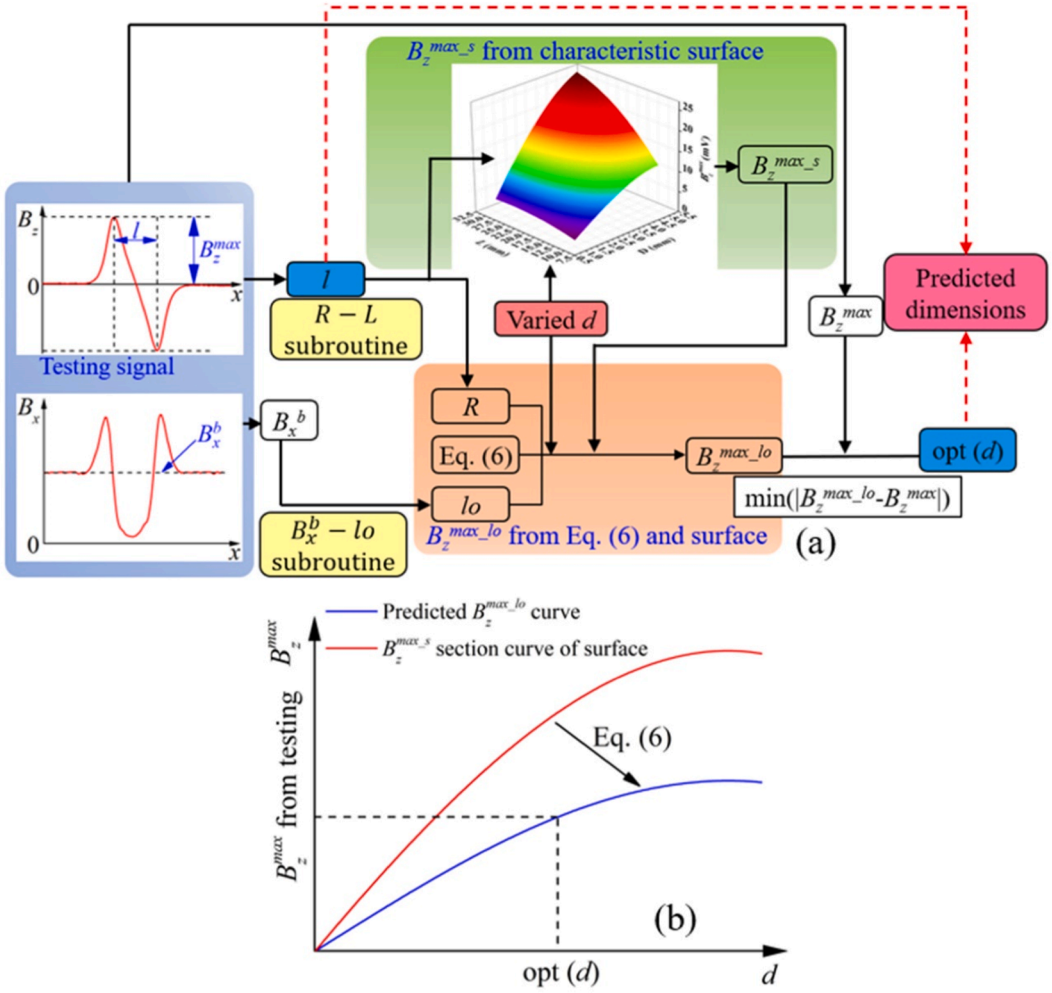

Fig. 3. (a) Diagram for the lift-off effect compensation algorithm. (b) Solution process of optimal d corresponding crack depth D.

only within the scope of depth D by a surface breaking crack. Namely, a current between 0 and crack depth D revolves around a certain vertical axis near the end of the crack, which leads to the peak and trough values of the B_z signal. D will be the upper limit of the algebraic integral of the vertical direction for the calculation of the deflecting electrical current around the axis.

2.2. Principle of lift-off effect compensation

According to Biot-Savart's law, the magnetic flux density $d\vec{B}$ is proportional to the current element $Id\vec{l}$ and inversely proportional to the square of the distance of interesting position from the current element. The magnetic flux density can be represented as Eq. (3).

$$d\vec{B} = \frac{\mu_0}{4\pi}\frac{Id\vec{l}\times\vec{r_0}}{r^2} \tag{3}$$

As shown in Fig. 2(a), a current I is applied to an unclosed ring whose radius is r, wrapping angle is φ, and center point is O. According to Eq. (3), the magnitude of the magnetic field density dB caused by the current element $Id\vec{l}$ can be given by Eq. (4).

$$dB = \frac{\mu_0 Idl}{4\pi(r^2+z^2)} \tag{4}$$

where z is the coordinate position along z-axis. The angle between the z-axis and the magnetic flux density $d\vec{B}$ is θ, and the integral magnetic field along the z-axis B_z can be written as Eq. (5). The direction of B_z is consistent with the positive z-axis.

$$B_z = \int_0^{\varphi} dB_z = \int_0^{\varphi} dB\cos\theta = \int_0^{\varphi}\frac{\mu_0 Idl}{4\pi(r^2+z^2)}\cos\theta = \frac{\varphi\mu_0 Ir^2}{4\pi(r^2+z^2)^{3/2}} \tag{5}$$

As shown in Fig. 2(b), the eddy current induced by the AC exciting coil is uniform in the conductive workpiece. The current rotates about the two points in the crack ends either clockwise or anticlockwise once it meets the crack. The magnetic density B_z is known to be produced by the crack-incurred deflecting part of J_y^z traveling along the $+z$ direction in a range of 0 to the crack depth D. Regarding the r direction, the limit of integration is from 0 to the equivalent radius R. The current of the element can be considered as $J_y^z \bullet drdz$ in the depth position of z, and the turning radius is r. The maximum value of B_z (B_z^{max}) in the P position can be represented using a double integral about J_y^z. According to Eq. (5), B_z^{max} is expressed as:

$$B_z^{max} = \frac{\varphi}{4\pi}\int_0^{D}\int_0^{R}\frac{\mu_0 J_y^0 \bullet e^{-z\sqrt{\pi f\mu\sigma}}\cos(\omega t - z\sqrt{\pi f\mu\sigma})\bullet r^2}{\left(\sqrt{r^2+(z+lo)^2}\right)^3}drdz \tag{6}$$

B_z^{max} is dependent on the crack depth D, the equivalent radius R and lift-off lo when the detected workpiece is determined (μ and σ are known). Eq. (6) indicates that B_z^{max} is a time-varying parameter. The root mean square (RMS) of B_z^{max} is always used in NDT practical applications for signal processing. Therefore, B_z^{max} is defined as the RMS of B_z^{max} in the following sections.

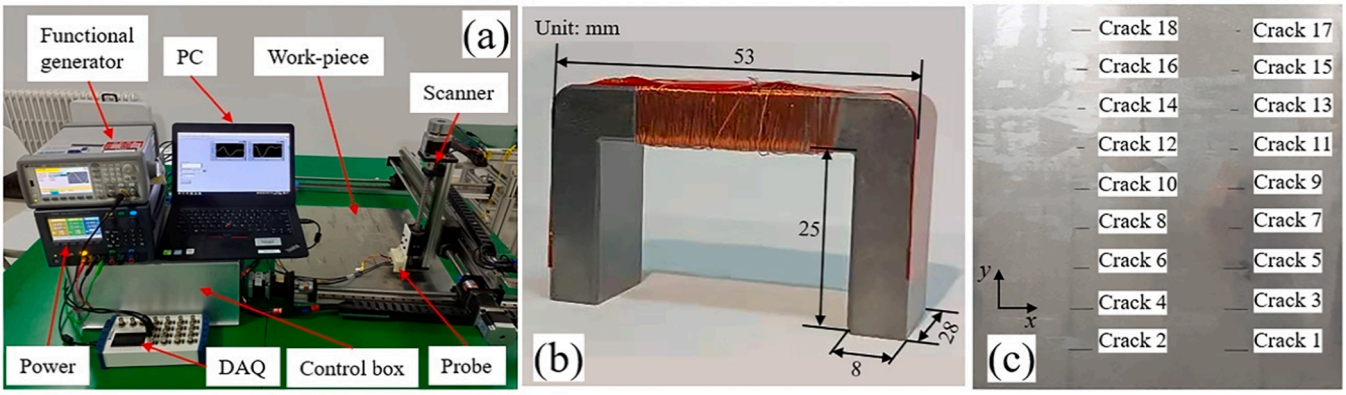

Fig. 4. (a) Photograph of ACFM detection system. (b) U-shaped yoke with coil. (c) Top-view of cracks on workpiece.

3. Crack sizing algorithm with unknown lift-off distance

3.1. Lift-off effect compensation algorithm

To reduce the influence of the lift-off effect in the ACFM system, we present a lift-off effect compensation algorithm, which can draw the profile of detected cracks at arbitrary lift-off distances. The diagram of the proposed algorithm is shown in Fig. 3(a).

First, the distance between the peak and trough of B_z testing signal l is obtained to present the crack length L. The value of l is almost constant and independent of the lift-off distance changes, so l can be utilized to indicate the crack length according to our previous work [19]. Additionally, the baseline of the B_x testing signal B_x^b can easily be acquired.

Second, a series of peak values of $B_z^{max\_s}$ with varied crack depth d (the red curve of Fig. 3(b)) can be obtained by a magnetic characteristic surface according to the length l obtained before. $B_z^{max\_s}$ is the data point in the magnetic characteristic surface. Moreover, $B_z^{max\_s}$ indicates the peak value of the B_z signal with different lengths (L) and depths (D) of a crack under a definite lift-off distance. The magnetic characteristic surface used to predict an unknown crack can be established by measuring the B_z signal with a fixed lift-off distance lo^f according to ref. [19]. The magnetic characteristic surface indicates the relationship between the peak of B_z (B_z^{max}), the length of crack L and the depth of crack D. The depth of the crack is set as a variable d, which is increased from 0 to the workpiece thickness with a very small step of constant Δd. When the length of the crack is known (l), the B_z^{max} - d variation curve with lift-off distance lo^f can be depicted. The curve is the intersection of the l vertical plane with the magnetic characteristic surface.

Third, a group of $B_z^{max\_lo}$, which is the peak strength of B_z curves with varied d, is acquired, which corresponds to the blue curve in Fig. 3(b). $B_z^{max\_lo}$ indicates the predicted peak value of the B_z signal under a certain lift-off distance (lo). The lift-off distance can be obtained in terms of the relationship between B_x^b and the lift-off distance lo. The equivalent radius R can be calculated by the R-L subprogram. Thus, the ratio of B_z^{max} with varied d under lo lift-off distance to under lo^f is directly obtained according to Eq. (6). B_z^{max} under a fixed lift-off distance lo^f has been determined by foregoing analysis, and $B_z^{max\_lo}$ under lo can easily be obtained.

Finally, the crack depth is calculated by a minimum value searching algorithm. The optimized d is considered the crack depth when the absolute difference between a certain $B_z^{max\_lo}$ and B_z^{max} detected by the B_z signal reaches the minimum, which is the core of the algorithm. The solution process of optimal d associated with crack depth D is shown in Fig. 3(b). The value of $\left|B_z^{max\_lo} - B_z^{max}\right|$ is very small and almost close to 0 when Δd is sufficiently small. Theoretically, d is the actual crack depth D when $B_z^{max\_lo}$ is equal to the B_z^{max} of the testing B_z curve.

Overall, there are three key procedures in this compensation algorithm, which is used to size the crack with an arbitrary lift-off distance. These procedures are the R solution, lo inference and the establishment of a magnetic characteristic surface using a z-axis magnetic signal.

3.2. ACFM detection system setup

Fig. 4(a) illustrates a photograph of the ACFM detection system. The critical part is a detection probe, which contains a U-shaped yoke wrapped with a 150-turn rectangle coil and a pair of tunneling magnetoresistance (TMR) sensor-based sensing units. In detail, the U-shaped yoke is made of Mn-Zn ferrite with a relative permeability (μ_r) of 7500, and the dimensions of the yoke are shown in Fig. 4(b); the coil is used to generate an AC magnetic field at a frequency of 3 kHz, and the driving signal is supplied by a functional generator (AFG1022, Tektronix, USA) with an amplitude of 42.3 mA; the sensing unit is designed to contain a high-pass filter with a cutoff frequency of over 100 Hz and gain factor of 100 × to detect the magnetic fields of B_x and B_z induced by the crack in the high-frequency range, and this unit is powered by a DC power supply (E36311A, Keysight, USA).

To verify our proposed algorithm, a series of 0.8 mm-wide (W) cracks was fabricated by electrical discharge machining (EDM) at the surface of a 500 mm × 500 mm × 6 mm 6061 aluminum workpiece, and the cracks were labeled No. 1 to No. 18. A top-view picture of the experimental workpiece is shown in Fig. 4(c). The dimensions of these cracks are summarized in Table 1.

During the test, the probe moved at a constant velocity of 50 mm/s along the crack longitudinal direction with different lift-off distances,

Table 1
Crack dimensions of workpiece.

Crack	1	2	3	4	5	6	7	8	9
L (mm)	30.00	30.00	30.00	30.00	30.00	20.00	20.00	20.00	20.00
D (mm)	5.00	4.00	3.00	2.00	1.00	5.00	4.00	3.00	2.00
W (mm)	0.80	0.80	0.80	0.80	0.80	0.80	0.80	0.80	0.80
Crack	10	11	12	13	14	15	16	17	18
L (mm)	20.00	10.00	10.00	10.00	10.00	10.00	15.00	5.00	25.00
D (mm)	1.00	5.00	4.00	3.00	2.00	1.00	5.00	5.00	5.00
W (mm)	0.80	0.80	0.80	0.80	0.80	0.80	0.80	0.80	0.80

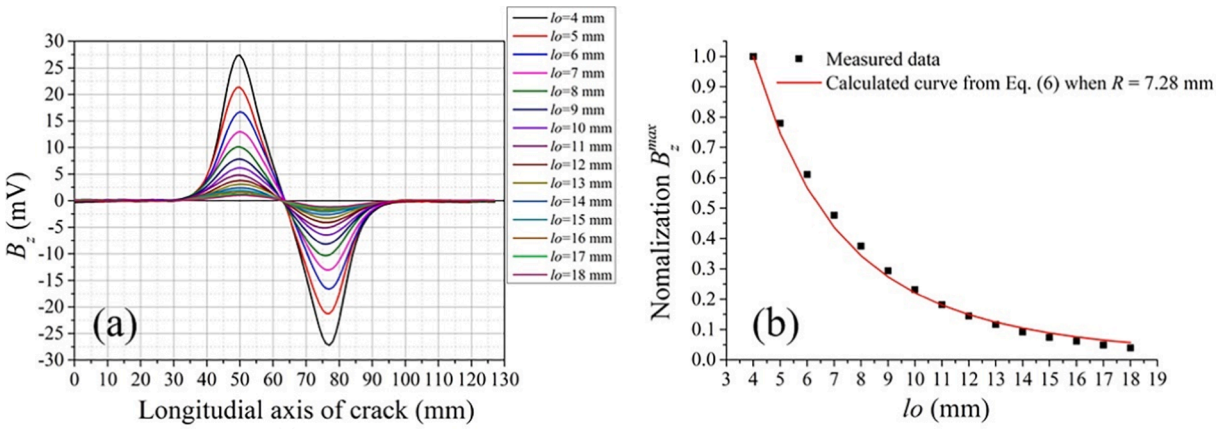

Fig. 5. (a) B_z magnetic signal at $L = 30$ mm, $D = 5$ mm and lift-off distance lo ranging from 4 to 18 mm with a step of 1 mm. (b) Normalization B_z^{max} variation in the experiment and in Eq. (6) with lift-off distance lo.

allowing the probe to pick up the interesting magnetic fields. The minimum lift-off distance lo^f is 4 mm due to the system limitation. Then, the output signals from the probe were captured by a data acquisition (DAQ) card (National Instrument, USA) and transferred to a PC by USB cable. All output signals were first denoised using a multiparameter synergy analysis (MPSA) algorithm [21,22] and then processed for crack inversion.

3.3. Equivalent radius

As mentioned above, the peak values of B_z signals appear on the ends of the detected crack. Thus, the length of the crack can be represented by the distance between two peaks. To obtain the value of equivalent radius, a series of B_z curves for the cracks with $L = 30$ mm and $D = 5$ mm are shown in Fig. 5(a). In this test, the lift-off distance was changed from 4 to 18 mm with an increment of 1 mm. From this figure, the peak value can be seen to decrease gradually as the lift-off distance increases. Moreover, the distances between two peaks (l in Fig. 3) of all curves are almost unchanged. The average value of l is 27.5 mm, which corresponds to a crack length of 30 mm. This result demonstrates that the peak-to-peak distance of the B_z signal is independent of the lift-off distance, so it can be used to evaluate the length of the crack directly without further calibration.

The B_z^{max} values of all B_z curves in Fig. 5(a) were extracted and normalized. The effects of unknown parameters φ, J_y^0 in Eq. (6) can be eliminated by normalizing, which was the ratio of B_z^{max} under all lift-off distances to under lo^f. The normalized B_z^{max} in Eq. (6) can be calculated in terms of the crack parameters and lift-off distance lo when R is known. The conductivity σ and relative permeability μ_r of the workpiece are 2.5 $\times$ 10^7 S/m and 1, respectively, which are used in Eq. (6). An iterative process was carried out to search for the optimal equivalent radius R. In this process, the initial value of R was 0, and the value increased by 0.01 mm at a time. Meanwhile, we define a stopping function to determine the R value, which is expressed as:

$$er^R = \sum_{lo=4}^{18} \left| B_z^{max\_lo} - B_z^{max\_lo'} \right|^2 \tag{7}$$

where $B_z^{max\_lo}$ and $B_z^{max\_lo'}$ are measured from the experiment and calculated from Eq. (6), respectively.

The optimized value of R is determined under the condition of the residual er^R in Eq. (7) reaching an acceptable tolerance. The trade-off er^R was set as 0.01 in our study for quick calculation. The experimental data and fitting curve of normalization B_z^{max} against lift-off distance lo from Eq. (6) are shown in Fig. 5(b). Through this method, the equivalent radius R was determined to be 7.28 mm when the iterative stopping condition was triggered.

Table 2
Equivalent radius R with different cracks.

Crack	L (mm)	D (mm)	R (mm)
1	30.00	5.00	7.28
2	30.00	4.00	7.31
3	30.00	3.00	7.30
4	30.00	2.00	7.32
5	30.00	1.00	7.29

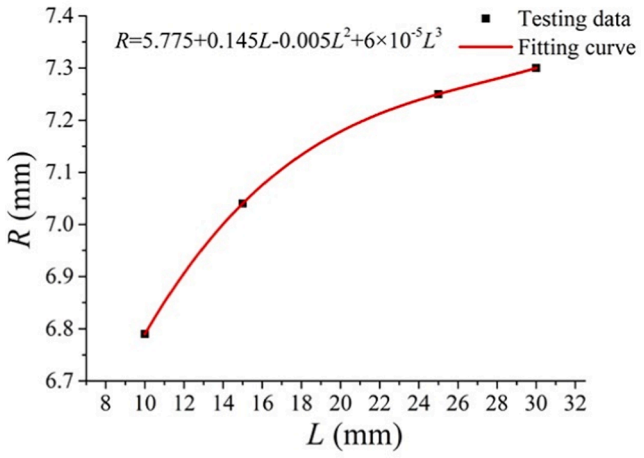

Fig. 6. Relationship between equivalent radius R crack length L.

First, the effect of depth on equivalent radius R was investigated with a fixed length of crack $L = 30$ mm. The measurements of B_z^{max} and error calculations of the first five cracks were conducted for the acquisition of the corresponding equivalent radius R, which is shown in Table 2. Clearly, R is independent of the depth of the crack. The average value of R is 7.30 mm at $L = 30$ mm.

Then, the effect of crack length was explored with the same depth of $D = 5$ mm, and the lengths were set at 10, 15, 25, and 30 mm. Particularly, the crack of $L = 20$ mm was excluded from the experimental sequence, because the crack of $L = 20$ mm would be used to validate our proposed method later. After calculating the R value for each case, the relationship between R and L is summarized in Fig. 6. The equivalent radius R can be expressed by a fitting polynomial equation as Eq. (8):

$$R = 5.775 + 0.145L - 0.005L^2 + 6 \times 10^{-5}L^3 \tag{8}$$

By using this equation, a supposed radius R can be derived directly

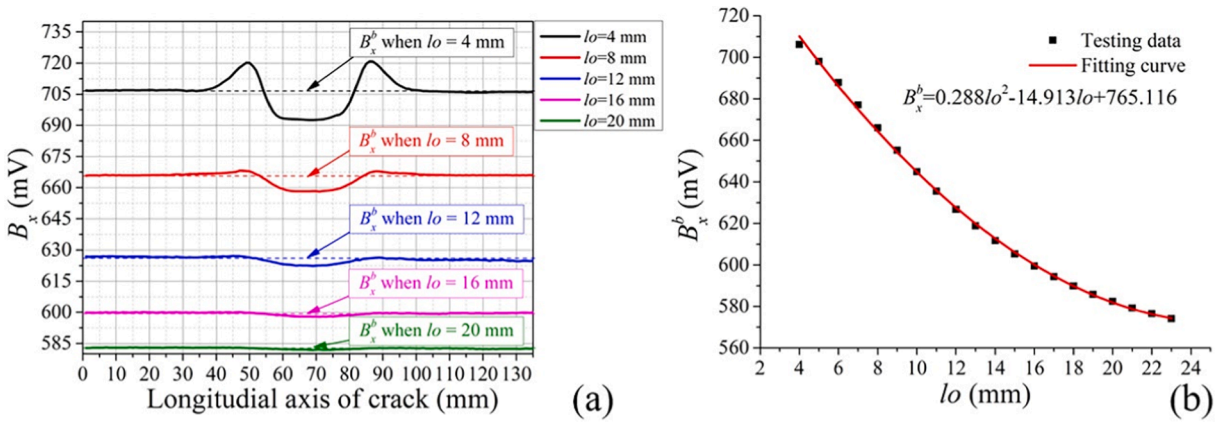

Fig. 7. (a) Testing magnetic signal B_x and B_x baseline $B_x{}^b$ at $L = 30$ mm, $D = 5$ mm and lo ranging from 4 to 20 mm with a step of 4 mm. (b) Relationship between B_x signal baseline $B_x{}^b$ and lift-off lo.

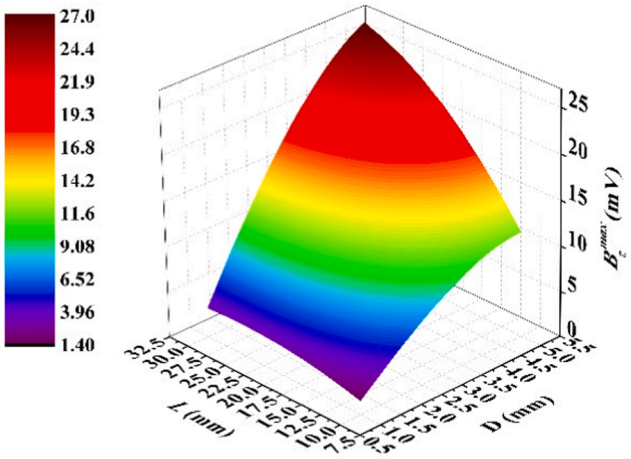

Fig. 8. Magnetic characteristic surface using testing data.

based on crack length L.

3.4. Lift-off distance prediction

The trough of the B_x signal results from the decrease in current on the metal surface; hence, it contains crack depth information. To characterize the lift-off effect on the trough of the B_x signal, a fixed crack length of $L = 30$ mm and crack depth of $D = 5$ mm (Crack 1) were investigated, as shown in Fig. 7(a). Clearly, the variance of B_x decreases sharply with increasing lift-off distance. Unlike the peak width of the B_z signal, the B_x signal is sensitive to the effect caused by the change in lift-off distance. It is hardly convincing that the depth of the crack is quantified directly using an inversion equation with a fixed lift-off distance, as in ref. [23].

An approximate horizontal line can be found in the B_x signal when the crack is absent, and it is labeled $B_x{}^b$ (see Fig. 7(a)). The lift-off effect on $B_x{}^b$ was also studied to obtain the relationship between $B_x{}^b$ and the lift-off distance lo. The values of $B_x{}^b$ with different lift-off distances were fitted by quadratic polynomial interpolation, as shown in Fig. 7 (b). $B_x{}^b$ decreases monotonically as the lift-off distance increases, and the fitting equation can be expressed as Eq. (9).

The lift-off distance in terms of the B_x signal from the detected flawless area can be predicted easily according to Eq. (9), which is the precondition of crack sizing with an unknown lift-off distance.

$$B_x^b = 0.288lo^2 - 14.913lo + 765.116 \tag{9}$$

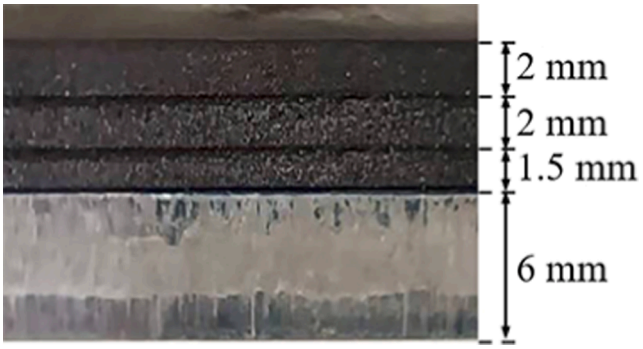

Fig. 9. Rubber pads covered with workpiece.

3.5. Magnetic characteristic surface

The B_z signals of cracks 1–15 at a lift-off distance of 4 mm were removed to build a magnetic characteristic polynomial surface. The method is similar to our previous work [19]. The characteristic surface is shown in Fig. 8, and the fitting equation is expressed in Eq. (10).

As mentioned above, the crack length L can be obtained directly from the B_z signal. When the lift-off distance was 4 mm, an intersection point was obtained on the characteristic surface according to the $B_z{}^{max}$ of the B_z signal, and then, the crack depth D was derived inversely from Eq. (10). In our iterative algorithm, d corresponding to crack depth is an iterative parameter, and l is the distance between two peaks of the B_z curve, equivalent to a section line of position l on the characteristic surface.

$$\begin{aligned} B_z^{max} = &-1.741 - 0.286D - 0.01948L + 0.3315D^2 + 0.4405DL \\ &- 0.003719L^2 - 0.0698D^3 - 0.01665D^2L - 0.0043DL^2 \end{aligned} \tag{10}$$

4. Method verification

To verify the performance of the proposed method, a validated experiment was carried out to estimate the dimensions of cracks with varied lift-off distances.

Three rubber pads were chosen to imitate a coating with different thicknesses. Three thicknesses, 1.5, 3.5 and 5.5 mm, were adopted in our experiment by combining pads on the aluminum plate. The inherent lift-off distance of the sensor is 4 mm in the probe, so the actual lift-off distances are 5.5, 7.5 and 9.5 mm. The experimental setup was the same as Fig. 4(a), and the workpiece was covered by three rubber pads simultaneously, as shown in Fig. 9.

Cracks 6, 10 and 17 were measured because they were not involved

Table 3
Testing results of crack dimensions.

Crack	lo (mm)	lo' (mm)	lo_{error} (%)	L (mm)	l (mm)	L_{error} (%)	D (mm)	d (mm)	D_{error} (%)
6	5.50	5.62	2.18	20.00	18.50	7.50	5.00	5.22	**4.40**
	7.50	7.56	0.80	20.00	18.70	6.50	5.00	5.32	**6.40**
	9.50	9.70	2.11	20.00	18.80	6.00	5.00	5.36	**7.20**
10	5.50	5.68	3.27	20.00	18.60	7.00	1.00	1.04	**4.00**
	7.50	7.60	1.33	20.00	18.80	6.00	1.00	1.07	**7.00**
	9.50	9.74	2.53	20.00	18.90	5.50	1.00	1.10	**10.00**
17	5.50	5.73	4.18	5.00	4.70	6.00	5.00	5.06	**1.20**
	7.50	7.58	1.07	5.00	4.90	2.00	5.00	5.46	**9.20**
	9.50	9.66	1.68	5.00	4.90	2.00	5.00	5.47	**9.40**

in the equivalent radius R calculation. The dimensions of these cracks are listed in Table 1. During measurement, each crack was repeated three times, and the average values of the tested data are summarized in Table 3. Moreover, the predicted depths of these cracks based on our algorithm were also demonstrated in Table 3. In Table 3, lo is actual lift-off distance; lo' is the predicted value of lift-off distance using the proposed method; lo_{error} is the predicted error of lift-off distance which is defined as $\frac{|lo'-lo|}{lo} \times 100\%$; L is the actual length of the crack; l is the predicted length of the crack; L_{error} is the predicted error of the crack length which is defined as $\frac{|L-l|}{L} \times 100\%$; D and d are the actual and predicted depth of the crack, respectively; D_{error} is the predicted error of crack depth which is defined as $\frac{|D-d|}{D} \times 100\%$. The lift-off distance prediction relative error of crack 17 is 4.18%, which is the maximum of all cracks. The relative errors of the length of all cracks decrease with increasing lift-off distance, but the relative errors of depth are the opposite. The maximum relative error of length is 7.50%, which corresponds to crack 6 at a 5.50 mm lift-off distance. As a whole, the relative errors of depths are larger than the relative errors of lengths. The maximum relative error of the depth of all cracks is 10.00%, which is the analyzed result of crack detection of crack 10 with a lift-off distance of 9.50 mm. Using the proposed algorithm, the relative errors of three parameters (lift-off distance, the length and depth of the crack) of all cracks with these three lift-off distances are no more than 10.00%, which is an acceptable error in NDT.

We can conclude that the dimensions (length and depth) of cracks at an unknown lift-off distance can be quantified for ACFM detection using our proposed method.

5. Conclusions

In this paper, we present a lift-off effect compensation algorithm based on an ACFM magnetic signal for crack sizing on an aluminum plate. The theoretical model was developed, and a mathematical expression was given. An ACFM testing system was set up to collect the B_x and B_z signals of cracks. The crack length was directly acquired by the peak width l of the B_z signal, which is immune to the lift-off distance. The equivalent radius R was obtained according to the relationship between R and crack length L. The lift-off distance was determined by the $B_x{}^b$ of the B_x signal. A $B_z{}^{max}$ interpolation surface was fitted with respect to the crack length L and depth D. The depth of the crack can be determined in terms of l, R and the magnetic characteristic surface. Finally, algorithm verification testing was carried out. The results demonstrate that the dimensions of cracks can be inferred, and the maximum relative error of depth is controlled within 10% by the lift-off compensation algorithm. Further work will focus on the development of a lift-off effect algorithm for ferromagnetic materials.

CRediT authorship contribution statement

Shuxiang Zhao: Writing – original draft, Conceptualization, Methodology, Software, Investigation. **Ying Shen:** Resources, Funding acquisition. **Lingsi Sun:** Validation. **Jiazeng Wang:** Software. **Zhineng Mao:** Validation. **Zhaoqiang Chu:** Data curation. **Jiamin Chen:** Data curation. **Junqi Gao:** Writing – review & editing, Resources, Funding acquisition.

Declaration of Competing Interest

The authors declare that they have no known competing financial interests or personal relationships that could have appeared to influence the work reported in this paper.

Acknowledgments

This work was supported by National Key R&D Program of China (Grant No. 2021YFB2011600), National Natural Science Foundation of China (Grant No. 62101151), Natural Science Foundation of Heilongjiang Province of China (Grant No. G3121054) and Natural Science Foundation of Shandong Province (Grant No. ZR2021MF106).

References

[1] B. Blakeley, M. Lugg, Recent research and development activities in electromagnetic sensor technologies, Insight: Non-Destructive Testing & Condition Monitoring 53 (3) (2011) 138–141,145.
[2] Lugg, M.C, Applications of A.C. Field Measurement Techniques for the Aircraft Industry, Aircraft Engineering & Aerospace Technology, 62 (1990) 9-11.
[3] M. Smith, C. Laenen, Inspection of nuclear storage tanks using remotely deployed ACFMT, Insight: Non-Destructive Testing & Condition Monitoring 49 (1) (2007) 17–20.
[4] J.M. Chacón Muñoz, F.P. García Márquez, M. Papaelias, Railroad inspection based on ACFM employing a non-uniform B-spline approach, Mech. Syst. Sig. Process. 40 (2013) 605–617.
[5] A. Raine, ASTM standard practice produced for the examination of welds using the alternating current field measurement (ACFM) technique, Insight - Non-Destructive Testing and Condition Monitoring 46 (2004) 44–47.
[6] G.M. Javier, G.G. Jaime, V.S. Ernesto, Non-destructive techniques based on eddy current testing, Sensors 11 (2011) 2525–2565.
[7] Y. Feng, L. Zhang, W. Zheng, Simulation analysis and experimental study of an alternating current field measurement probe for pipeline inner inspection, NDT and E Int. 98 (2018) 123–129.
[8] X.a. Yuan, W. Li, G. Chen, X. Yin, W. Jiang, J. Zhao, J. Ge, Inspection of both inner and outer cracks in aluminum tubes using double frequency circumferential current field testing method, Mechanical Systems and Signal Processing, 127 (2019) 16-34.
[9] J. Ge, B. Hu, C. Yang, Investigation of the approximate decomposition of alternating current field measurement signals from crack colonies, Mech. Syst. Sig. Process. 160 (2021), 107878.
[10] G.L. Nicholson, C.L. Davis, Modelling of the response of an ACFM sensor to rail and rail wheel RCF cracks, NDT and E Int. 46 (2012) 107–114.
[11] J.L. Shen, L. Zhou, H. Rowshandel, G.L. Nicholson, C.L. Davis, Determining the propagation angle for non-vertical surface-breaking cracks and its effect on crack sizing using an ACFM sensor, Meas. Sci. Technol. 26 (11) (2015) 115604.
[12] C.F. Ye, Y. Huang, L. Udpa, S.S. Udpa, Novel Rotating Current Probe With GMR Array Sensors for Steam Generate Tube Inspection, IEEE Sens. J. 16 (2016) 4995–5002.
[13] H. Rowshandel, G.L. Nicholson, J.L. Shen, C.L. Davis, Characterisation of clustered cracks using an ACFM sensor and application of an artificial neural network, NDT and E Int. 98 (2018) 80–88.
[14] S. Zhao, Y. Shen, J. Wang, R. Zhu, W. Zhai, H. Dong, Z. Mao, J. Gao, Extreme learning machine based sub-surface crack detection and quantification method for ACFM, J. Magn. Magn. Mater. 546 (2022), 168865.

[15] G.Y. Tian, A. Sophian, Reduction of lift-off effects for pulsed eddy current NDT, NDT and E Int. 38 (2005) 319–324.
[16] Y. Yu, Y. Yan, F. Wang, G. Tian, D. Zhang, An approach to reduce lift-off noise in pulsed eddy current nondestructive technology, NDT and E Int. 63 (2014) 1–6.
[17] M. Fan, B. Cao, P. Yang, W. Li, G. Tian, Elimination of liftoff effect using a model-based method for eddy current characterization of a plate, NDT and E Int. 74 (2015) 66–71.
[18] R.K. Amineh, M. Ravan, S.H.H. Sadeghi, R. Moini, Using AC field measurement data at an arbitrary liftoff distance to size long surface-breaking cracks in ferrous metals, NDT and E Int. 41 (2008) 169–177.
[19] S. Zhao, L. Sun, J. Gao, J. Wang, Y. Shen, Uniaxial ACFM detection system for metal crack size estimation using magnetic signature waveform analysis, Measurement 164 (2020), 108090.
[20] W.H. Hayt, J.A. Buck, Engineering Electromagnetics, 8th ed., McGraw-Hill Companies Inc., New York, 2012.
[21] J.Q. Gao, L.S. Sun, S.X. Zhao, Y. Shen, Enhanced ACFM detection performance by multi-parameter synergy analysis, Insight - Non-Destructive Testing and Condition Monitoring 62 (2020) 81–85.
[22] L. Sun, S. Zhao, Y. Shen, J. Wang, J. Gao, A performance improved ACFM-TMR detection system with tradeoff denoising algorithm, J. Magn. Magn. Mater. 527 (2021), 167756.
[23] X. Yuan, W. Li, G. Chen, X. Yin, W. Yang, J. Ge, Two-Step Interpolation Algorithm for Measurement of Longitudinal Cracks on Pipe Strings Using Circumferential Current Field Testing System, IEEE Trans. Ind. Inf. 14 (2018) 394–402.